Transdifferentiation of glioblastoma cells into vascular endothelial cells

Yasushi Soda[a], Tomotoshi Marumoto[a,b], Dinorah Friedmann-Morvinski[a], Mie Soda[a], Fei Liu[a], Hiroyuki Michiue[c], Sandra Pastorino[d], Meng Yang[e], Robert M. Hoffman[e,f], Santosh Kesari[d], and Inder M. Verma[a,1]

[a]Laboratory of Genetics, Salk Institute for Biological Studies, La Jolla, CA 92037; [b]Division of Molecular and Clinical Genetics, Department of Molecular Genetics, Medical Institute of Bioregulation, Kyushu University, Higashi-ku, Fukuoka 812-8582, Japan; [c]Department of Physiology, Okayama University Graduate School of Medicine, Dentistry, and Pharmaceutical Sciences, Okayama 700-8558, Japan; [d]Department of Neurosciences, Moore's Cancer Center, University of California at San Diego, La Jolla, CA 92093; [e]AntiCancer, Inc., San Diego, CA 92111; and [f]Department of Surgery, University of California at San Diego, San Diego, CA 92103

This Feature Article is part of a series identified by the Editorial Board as reporting findings of exceptional significance.

Edited by Douglas Hanahan, Swiss Institute for Experimental Cancer Research and Swiss Federal Institute of Technology Lausanne, Lausanne, Switzerland, and approved December 27, 2010 (received for review October 26, 2010)

Glioblastoma (GBM) is the most malignant brain tumor and is highly resistant to intensive combination therapies and anti-VEGF therapies. To assess the resistance mechanism to anti-VEGF therapy, we examined the vessels of GBMs in tumors that were induced by the transduction of $p53^{+/-}$ heterozygous mice with lentiviral vectors containing oncogenes and the marker GFP in the hippocampus of GFAP-Cre recombinase (Cre) mice. We were surprised to observe GFP^+ vascular endothelial cells (ECs). Transplantation of mouse GBM cells revealed that the tumor-derived endothelial cells (TDECs) originated from tumor-initiating cells and did not result from cell fusion of ECs and tumor cells. An in vitro differentiation assay suggested that hypoxia is an important factor in the differentiation of tumor cells to ECs and is independent of VEGF. TDEC formation was not only resistant to an anti-VEGF receptor inhibitor in mouse GBMs but it led to an increase in their frequency. A xenograft model of human GBM spheres from clinical specimens and direct clinical samples from patients with GBM also showed the presence of TDECs. We suggest that the TDEC is an important player in the resistance to anti-VEGF therapy, and hence a potential target for GBM therapy.

mouse model | glioma | angiogenesis | hypoxia-inducible factor 1

Glioblastoma multiforme (GBM) is the most common and lethal form of brain cancer. Despite optimal treatment and evolving standard of care, the median survival of patients diagnosed with GBM is only 12–15 mo (1). Because GBM is one of the most vascular-rich tumors and VEGF is produced by tumor cells, the anti-VEGF antibody bevacizumab (Avastin) is being used in clinical trials (2). In a phase II clinical trial, more than half of the patients with GBM responded to the combination treatment of bevacizumab and irinotecan, but this effect was transient in most patients (3). Mechanisms proposed to explain resistance to anti-VEGF therapy include activation of other proangiogenic signaling pathways, recruitment of bone marrow (BM)-derived myeloid cells that protect and nurture vascular cells, protection of blood vessels by increased pericyte coverage, and increased tumor invasion (4, 5). In GBMs, the antitumor effect of the antiangiogenic therapies is likely attributable to normalization of vasculature, which also decreases edema (3, 6). Recent studies have shown that tumor cells become more aggressive after antiangiogenic therapy (7).

The tumor vessels in GBMs are different from normal blood vessels morphologically and functionally. As with other tumors, the tumor vessels in GBMs are tortuous; disorganized; highly permeable; and abnormal in the endothelial walls, pericyte coverage, and basement membrane, resulting in loss of the blood–brain barrier (2). In addition, angiogenesis in GBMs has a unique feature, so-called "glomeruloid tufts," exhibiting aggressive proliferation of endothelial cells (ECs) compared with those of anaplastic glioma (grade III) (2). Recently, the possibility of EC differentiation of tumor cells has been suggested in lymphoma, myeloma, chronic myeloid leukemia (CML), breast cancer, and neuroblastoma (8–12). Therefore, we surmised that the mechanism of vascular formation in GBM may also be different from that of regular tumor vascular formation.

To investigate angiogenesis in GBMs, we examined our recent mouse GBM model in which tumors developed 2–6 mo after injection with viral vectors. The tumors showed all the features of GBM, including hypervascularity (13). Furthermore, tumors were GFP^+, because the vectors contained GFP in addition to activated oncogenes and loss of p53. Interestingly, in these tumors, we found many GFP^+ cells with EC characteristics, particularly in the deep area of the lesions, by confocal microscopy and flow cytometry, indicating the presence of tumor-derived endothelial cells (TDECs). Here, we demonstrate that the TDECs originated from tumor-initiating cells but not from contaminated EC progenitors or cell-to-cell fusion between tumor cells and ECs. The TDECs are functional because blood flows through them. Additionally, it has been suggested that hypoxia-inducible factor 1 (HIF-1) is an important enhancer of EC differentiation of tumor cells and that the formation of TDECs is independent of VEGF. Finally, direct clinical samples from patients show EC cells with tumor markers. Our report shows direct evidence of TDEC formation in GBMs, which may play a role in the resistance to anti-VEGF therapy.

Results

ECs Express Tumor-Specific Marker in Mouse GBM Models. To investigate angiogenesis in GBMs, we used our recent mouse GBM model (13). As previously reported, Cre recombinase (Cre)-loxP–controlled lentiviral vectors encoding the activated form of oncogenes H-Ras and Akt [pTomo vectors (13)] were injected stereotaxically into the hippocampus of GFAP-Cre-$p53^{+/-}$ mice. In this model, the oncogenes were expressed specifically in $GFAP^+$ cells and tumors expressed GFP, H-Ras, and Akt and showed loss of p53. Additionally, they were positive for the neural progenitor cell marker nestin, which is often expressed in human GBMs (14). To investigate the tumor vasculature, we carried out immunofluorescence by confocal microscopy using the endothelial antigens von Willebrand factor (vWF), CD31, CD34, and vascular endothelium (VE)-cadherin (CD144) as markers. Fig. 1*A* shows a normal EC, where the GFP

Author contributions: Y.S. and I.M.V. designed research; Y.S., T.M., D.F.-M., M.S., F.L., and H.M. performed research; S.P., M.Y., R.M.H., and S.K. contributed new reagents/analytic tools; Y.S., D.F.-M., and I.M.V. analyzed data; and Y.S., D.F.-M., S.K., and I.M.V. wrote paper.

The authors declare no conflict of interest.

This article is a PNAS Direct Submission.

See Commentary on page 4271.

[1]To whom correspondence should be addressed. E-mail: verma@salk.edu.

This article contains supporting information online at www.pnas.org/lookup/suppl/doi:10.1073/pnas.1016030108/-/DCSupplemental.

in tumor cells is completely distinct from vWF, the endothelial antigen (Fig. 1*A*, *i–iii*). Surprisingly, we found that some ECs expressed not only endothelial antigens but also GFP, which most likely originated from tumor cells (Fig. 1*B*, *i–iii*, compare with the merge in Fig. 1 *A*, *iii*, and *B*, *iii*, and Fig. S1A). Additionally some GFP$^+$ ECs formed vessels with GFP$^-$ regular ECs, exhibiting a mosaic pattern [Fig. 1*B*, *iv–vi*; a *z*-series assay further confirmed the mosaic pattern (Fig. S1*A*)]. Immunofluorescence with other EC-specific antigens like CD34 and CD144 also showed EC cells containing GFP, further supporting the formation of TDECs (Fig. *1B*, *vii–xii*). The GFP$^+$ ECs expressed the transduced oncogene Flag-tagged H-RasV12 (Fig. 1*C*, *i–v*). Similar results were obtained with HA-tagged Akt. Nestin expressed in tumor cells can be detected in both GFP$^+$ EC cells (marked T) and GFP$^-$ EC cells (marked R), further strengthening the notion that GFP$^+$ ECs (TDECs) most likely originated from the tumor cells (Fig. 1*C vi–x*). The TDECs were also observed when GBM was generated using lentivectors (LVs) containing only activated H-Ras and small interfering p53 (sip53). To confirm the presence of GFP$^+$ ECs, we also examined dissociated tumors by flow cytometry. Similar to the results of confocal microscopy, 10–25% of ECs (CD45$^-$CD31$^+$CD34$^+$) were positive for GFP (Fig. 1*D*). The TDECs were mostly found in the deep part of the tumor rather than on its surface, and the frequency of vessels containing the GFP$^+$ ECs was 6.4–37.8% (average of 24.6 ± 12.7%) in the deep area, depending on the size of the tumor. In the surface area, 2.0–12.7% (average of 8.33 ± 4.15%) of vessels contained the GFP$^+$ ECs (Table S1). In general, the frequency of the TDECs was higher in large tumors than in smaller tumors. By injecting Hypoxyprobe-1 (Natural Pharmacia International) into tail veins of tumor-harboring mice, we showed that the deep area of the tumor was more hypoxic than the surface area (Fig. 2*A*), suggesting that hypoxia may be an important factor for TDEC formation. Hypoxia leads to angiogenesis by induction of VEGF through increasing levels of HIF-1. Furthermore, tumors produced VEGF (13, 15). We are now pursuing HIF-1 expression by immunofluorescence studies. Interestingly, the majority of TDECs did not express VEGF receptor 2 (R2) (Fig. 2*B*, *vi–x*), whereas most of the regular ECs (GFP$^-$) expressed VEGF-R2 (Fig. 2*B*, *i–v*). The TDECs also did not show expression of VEGF-R1 and VEGF-R3. Because FGF-2 is another important growth factor expressed by the ECs and the GBM cells, we also examined the expression of FGF receptor 1 (FGFR-1). In contrast to the results of VEGF receptors, the FGFR-1 was expressed in both TDECs (marked T) and regular ECs (marked R) as well as in surrounding tumor cells (Fig. 2*C*).

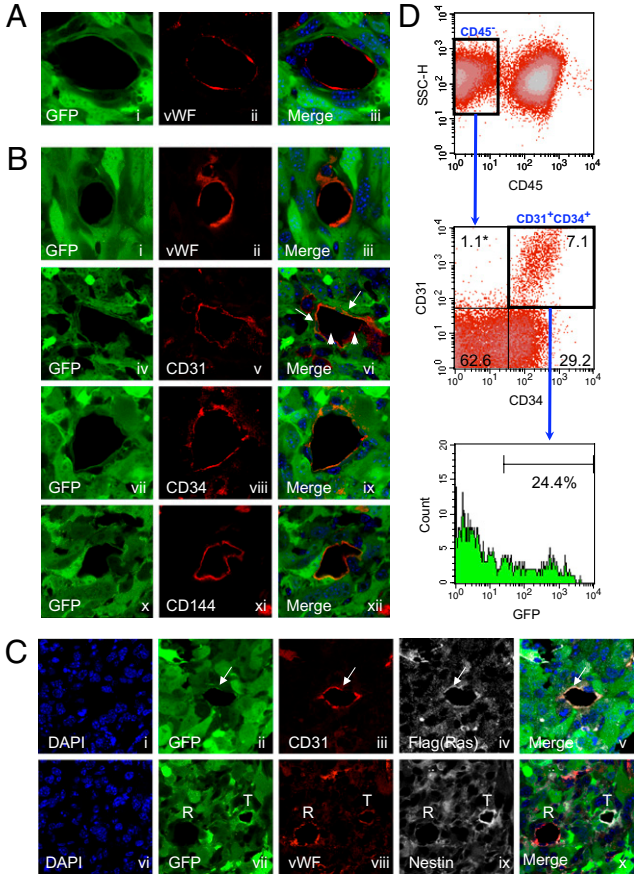

Fig. 1. TDECs. GFAP-Cre/p53$^{+/-}$ mouse brain was transduced by Tomo H-RasV12 LVs and Tomo Akt LVs as described (13). A representative image of ECs observed by confocal microscopy is shown. (*A*) Regular ECs lined the vessel lumen and expressed EC marker vWF (*ii*) but not the tumor marker GFP (*i*). DAPI was used as the nuclear marker, and the image was incorporated in the merge panel (*iii*). (*B*) In contrast, TDECs expressed both the GFP marker (*i, iv, vii*, and *x*) and EC markers vWF (*ii*), CD31 (*v*), CD34 (*viii*), and CD144 (*xi*). Some GFP$^+$ ECs formed vessels with GFP$^-$ regular ECs (*vi*, arrowheads). DAPI was used as the nuclear marker, and the image was incorporated in the merge panels (*iii, vi, ix*, and *xii*). (*C*) TDECs expressed Flag-tagged H-RasV12 in addition to GFP and CD31 (*i–v*, arrows). They also expressed nestin in addition to GFP and vWF (*vi–x*, R and T indicate regular ECs and TDECs, respectively). (*D*) Representative result of flow cytometry for dissociated brain tumors. In the CD45$^-$ population (*Top*), ECs were CD31$^+$CD34$^+$ and constituted 7.1% of the whole tumor (*Middle*) and GFP$^+$ ECs (TDECs) represented 24.4% of total ECs (*Bottom*). The asterisk represents the percentage of cells in each quadrant. All confocal pictures are single-slice images at an Airy factor of 1.0. [Magnification: all confocal images were taken at 63× with 3× (*A* and *B*) or 2× (*C*) electrical zoom (total magnification: 189× or 126×).]

TDEC-Forming Vessels Are Functional. To assess if TDECs are functional, we determined blood flow in TDEC-containing vessels. We injected biotinylated lectin i.v., which can bind to ECs in mice harboring brain tumors, 15 min before euthanasia. To

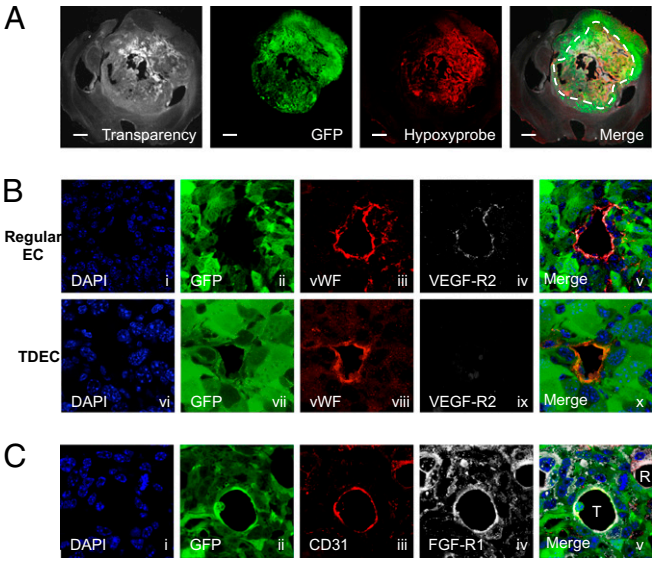

Fig. 2. Hypoxia and expression of HIF-1α and receptors of angiogenic growth factors. (*A*) Hypoxyprobe assay of the tumor. The hypoxic area ($p0_2$ < 10 mmHg) was detected by the anti-Hypoxyprobe antibody. The dotted line shows the approximate border of the hypoxic area. (Scale bar: 1 mm.) (*B*) Regular tumor ECs expressed VEGF-R2 (*i–v*), but GFP$^+$ TDECs did not express VEGF-R2 (*vi–x*). (*C*) GFP$^+$ TDECs (T) expressed FGF-R1, as did regular ECs (R) and surrounding tumor cells. All confocal pictures are single-slice images at an Airy factor of 1.0. [Magnification: 63× with 3× electrical zoom (total magnification: 189×) except *A*, which was 1.25×.]

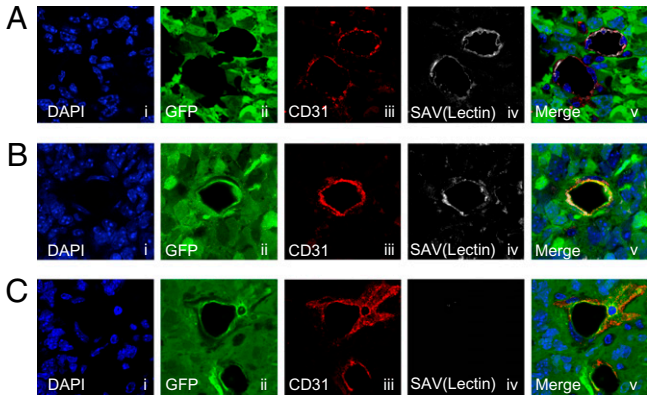

Fig. 3. Blood flow in TDEC-forming vessels. Biotinylated lectin injection assay showed that both regular vessels (*A*) and TDEC-forming vessels (*B*) are functional and allowed blood flow. (*C*) Nonfunctional TDEC-forming vessels were also observed. All confocal pictures are single-slice images at an Airy factor of 1.0. [Magnification: 63× with 3× electrical zoom (total magnification: 189×).]

visualize the blood flow, tumor sections were stained with fluorescence-labeled streptavidin, which binds to biotinylated lectin-labeled ECs. Just like regular ECs, lectin-bound TDECs were observed in many tumors, indicating that the TDEC-forming vessels are functional (Fig. 3 *A* and *B*). There were also nonfunctional TDEC-forming vessels (Fig. 3*C*).

TDECs in Transplanted Tumors. We next investigated the ability of tumor cells to differentiate into ECs by transplanting mouse GBM cell line 005, which is a tumor-initiating cell line established from our lentiviral vector-induced tumor model, into the brain of a nonobese diabetic (NOD)-SCID mouse. On examination of the tumor vessels in the transplanted mice, GFP^+ ECs were observed (Fig. 4*A*, *i–iv*). We further established 14 subclones of the 005 cells and transplanted them into NOD-SCID mouse brains. Most clones formed tumors in the same way as the parental 005 cells and contained GFP^+ ECs in these tumors. Data from one such subclone are shown using CD34 as a marker of ECs (Fig. 4*B*, *i–iv*). Because it has been reported that some $GFAP^+$ neural stem cells (NSCs) can transdifferentiate into ECs (16), it is possible that 005 cells may contain transduced $GFAP^+$ NSCs in addition to tumor-initiating cells and that these $GFAP^+$ NSCs differentiate into the GFP^+ ECs. We therefore generated a cell line from another tumor (006) induced by pTomo vector. Results from 006 cells also show GFP^+ ECs (Fig. 4*C*, *i–iv*), thus minimizing the possibility of the presence of $GFAP^+$ NSCs in tumor-initiating cells that differentiated into the ECs.

Fusion-Independent Mechanism in TDEC Formation. To exclude the possibility that GFP^+ ECs (TDECs) result from cell fusion of tumor cells and ECs but are not derived from tumor cells, we transplanted 005 tumor cells into the brains of DsRed-transgenic nude mice and examined the expression of GFP, DsRed, and EC markers in the transplanted tumors. In these transgenic mice, the DsRed is driven by the CAG promoter and all cell types except hair and red blood cells express DsRed (17). In tumors developed in these mice, many $DsRed^+$ host cells, including ECs, were infiltrating into the tumors (Fig. S1*B*). Confocal microscopy revealed that GFP^- ECs were expressing DsRed (Fig. 4*D*, *i–iv*), whereas GFP^+ ECs were not expressing DsRed (Fig. 4*D*, *v–viii*), thus confirming that the GFP^+ TDECs were derived from a fusion-independent mechanism. To confirm these results, we also examined dissociated tumors by flow cytometry. Similar to the results of confocal microscopy, most of the GFP^+ ECs were $DsRed^-$, whereas $DsRed^+$ ECs were GFP^- (Fig. 4*E*). We further examined the cell fusion in the NOD-SCID mouse transplantation model by flow cytometry. In this model, MHC class I $H\text{-}2K^d$ is expressed in the host cells but not in 005-derived tumor cells.

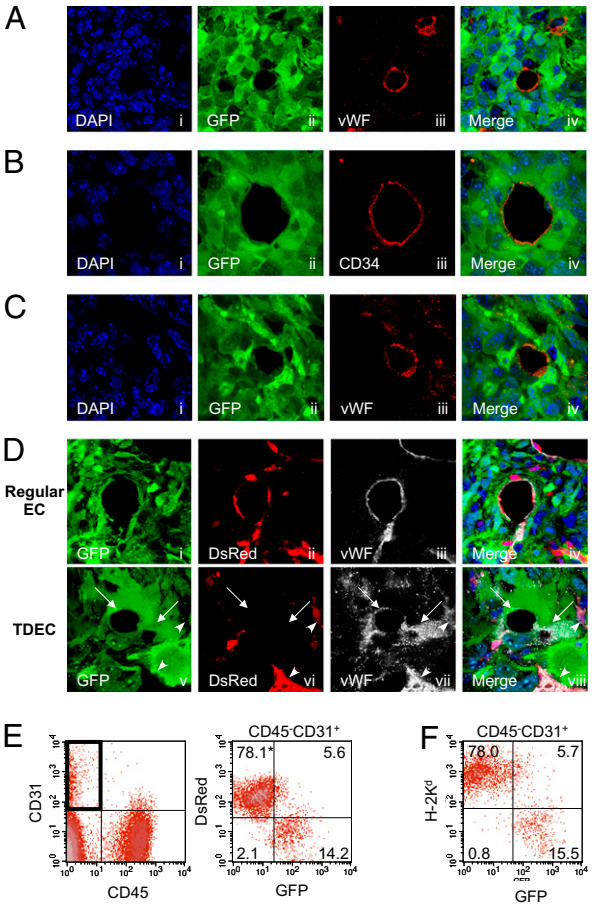

Fig. 4. TDECs in tumor-initiating cells transplanted into immunocompromised mice. Representative images of TDECs in brain tumors developed in NOD-SCID mice transplanted with tumor-initiating cell line. Cell line 005 (*A*), 005 subclone cells (*B*), and another tumor-initiating cell line 006 (*C*). TDECs expressed GFP and EC markers vWF and CD34. (*D*) Representative image of regular ECs and TDECs in brain tumors developed in DsRed nude mice transplanted with 005 cells by confocal microscopy. Regular tumor vessel ECs expressed vWF and host marker DsRed but not tumor marker GFP (*i–iv*), whereas GFP^+ vWF^+ TDECs did not express DsRed (*v–viii*). TDECs are indicated by arrows, and regular ECs are indicated by arrowheads (*v–viii*). All confocal pictures are single-slice images at an Airy factor of 1.0. [Magnification: 63× with 3× electrical zoom (total magnification: 189×).] (*E*) Representative results of flow cytometry of dissociated tumors developed in DsRed nude mice transplanted with 005 subclone cells. In the $CD45^-CD31^+$ EC fraction (*Left*), DsRed-positive cells did not express GFP (*Right*). (*F*) Representative results of flow cytometry for dissociated tumors developed in NOD-SCID mice. In the $CD45^-CD31^+$ EC fraction, cells expressing NOD-SCID mouse-specific $H\text{-}2K^d$ did not express GFP. The asterisk represents the percentage of cells in each quadrant.

The majority of $H\text{-}2K^{d+}$ host-derived ECs were GFP^-, whereas GFP^+ ECs were $H\text{-}2Kd^-$ (Fig. 4*F*), again suggesting a fusion-independent mechanism of TDEC formation.

In Vitro Differentiation of GBM Cells to ECs: Role of Hypoxia and HIF-1. We next attempted to induce GBM initiating cells (005 cells) to differentiate into ECs in vitro. Because HIF-1 is likely to be an important factor for TDEC formation, we added an iron chelator, deferoxamine (DFO), into the culture media to mimic hypoxic conditions by blocking proline hydroxylase (18, 19), which stabilizes HIF-1α. Culturing 005 cells in DMEM/F-12 medium supplemented with FBS (DFS) and endothelial cell growth medium (EGM; Lonza), which contains FBS, human VEGF, human EGF, human FGF-2, insulin-like growth factor, cortisol, and heparin, induced significant morphological changes. DFO en-

hanced the change to endothelial-like morphology in DFS medium or EGM but not in N2 medium, which is used to maintain the NSCs (Fig. 5*A*). In the DFS medium and EGM, DFO significantly enhanced the HIF-1α expression in the 005 cells (Fig. 5*B*) and induced expression of endothelial antigens vWF and CD31 (Fig. 5 *C* and *D*). However, VEGF-R2 expression was induced only in a small population of cells (Fig. 5*D*). Additionally, these differentiated cells formed a tube structure on Matrigel (Becton Dickinson) (Fig. 5*E*). To confirm that this endothelial differentiation results from HIF-1α accumulation but not from a nonspecific effect of DFO, we cultured the 005 cells in 2% O_2 (hypoxia). Tubular structures could be observed in the absence of DFO when these cells were cultured in DFS medium or EGM but not in N2 medium (Fig. 5*E*), suggesting that hypoxia, presumably through the activation of HIF-1 α (Fig. 5*B*), is playing an important role in the endothelial differentiation.

VEGF-Independent Transdifferentiation of Tumor Cells. Because VEGF is a critical factor in tumor angiogenesis and is induced by hypoxia through accumulation of HIF-1α (15), we investigated the role of VEGF in the formation of TDECs. VEGF was released constitutively from 005 cells in N2 medium at a low level (32.2 ± 8.8 pg/mL per 10^6 cells), and the amount of VEGF release increased about threefold in DFS medium and EGM. In the presence of DFO, however, secretion of VEGF in both DFS medium (243 ± 22.2 pg/mL) and EGM (368 ± 32.6 pg/mL) was significantly increased. No effect was observed in N2 medium (Fig. 6*A*). These results suggest that VEGF may play a role in endothelial differentiation of 005 cells. We therefore blocked autocrine VEGF function with anti-mouse VEGF neutralization antibody (NAb) in addition to using EGM devoid of human VEGF. Tube formation of 005 cells cultured in DFS with DFO medium or in EGM with or without DFO was not inhibited at all despite the addition of 1 μg/mL NAb (Fig. 6*B*), which completely inhibited activity of 100 ng/mL VEGF on growth of human umbilical vein endothelial cells (HUVECs), whereas 10 ng/mL VEGF can enhance tube formation of HUVECs (Fig. S2). We also added the anti-VEGF receptor–specific small molecule inhibitor AG28262 (Pfizer), which inhibits autophosphorylation of VEGF-R1, VEGF-R2, and VEGF-R3 selectively at a subnanomolar concentration (20). There was no inhibition of tube formation even at a 20-nM concentration of the inhibitor (Fig. 6*C*). Because the TDECs were expressing FGFR-1 in our mouse GBMs (Fig. 2*D*), we used a high concentration of the AG28262 (200 and 1,000 nM), which inhibits not only VEGF receptors but FGFR-1. However, there was no significant inhibition of tube formation (Fig. 6*C*). These results reaffirm that GBM-initiating cells are able to differentiate into ECs by a VEGF- or FGF-independent mechanism.

Resistance of TDECs to Anti-VEGF Receptor Inhibitor. To confirm the resistance of TDECs to anti-VEGF therapies and that this resistance is playing an important role in the resistance of patients

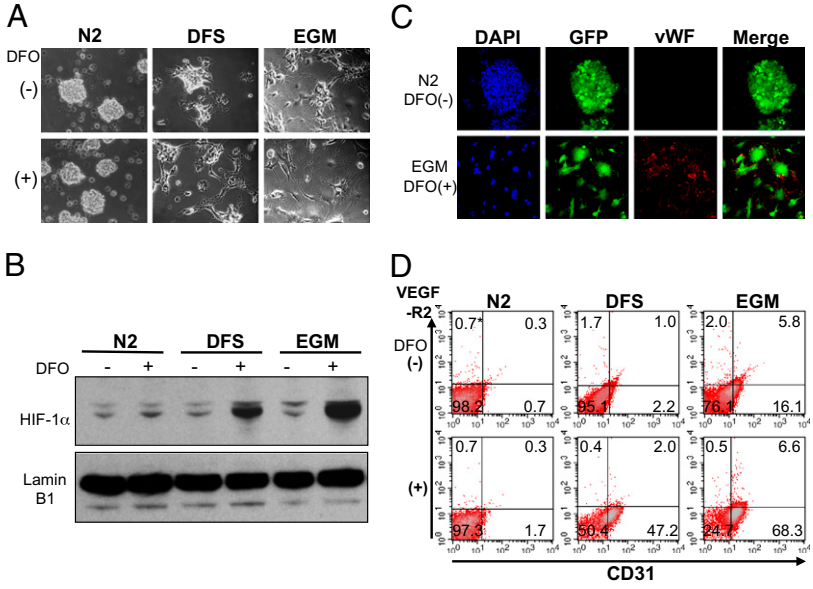

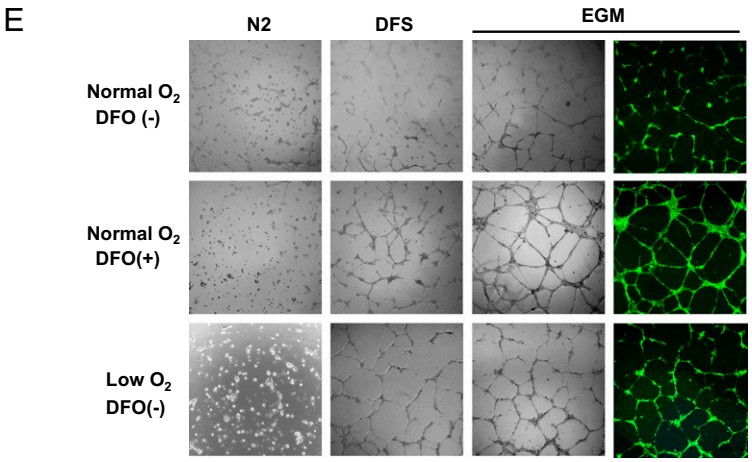

Fig. 5. Endothelial differentiation of tumor-initiating cells in vitro. (*A*) Morphological changes of 005 cells cultured in N2 medium, DFS medium, and EGM with or without DFO. (*B*) Expression of HIF-1α in 005 cells cultured in the indicated conditions. Nuclear protein was extracted from the cells and analyzed by Western blotting using anti-HIF-1α antibody (*Upper*) or anti-lamin B1 antibody (*Lower*). (*C*) Representative confocal microscopy images of 005 cells cultured in N2 medium without DFO (*Upper*) or in EGM with DFO (*Lower*). The confocal microscopy images are maximum projection images of consecutive single-slice images at an Airy factor of 1.0. (Magnification: 40×.) (*D*) Flow cytometry of CD31 and VEGF-R2 expression in 005 cells cultured in various conditions. (*E*) Tube formation assay of 005 cells cultured in the indicated conditions and seeded on Matrigel. The 005 cells were cultured in DFS medium with DFO and in EGM with or without DFO under normoxia-formed tube structure, and all these cells were GFP^+. The hypoxic condition (low O_2) in DFS medium and EGM without DFO also induced tube formation.

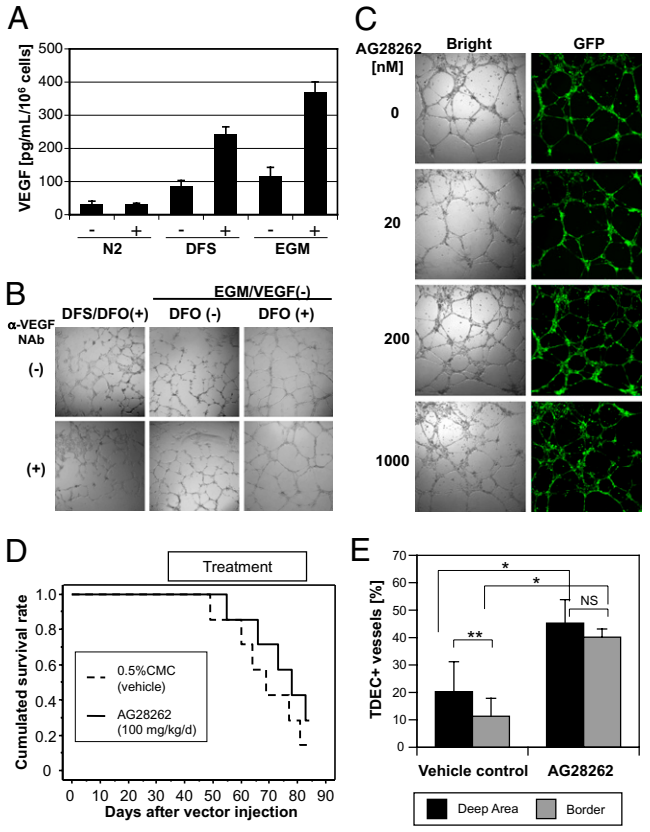

Fig. 6. Effect of inhibition of VEGF on TDEC formation. (*A*) Concentration of mVEGF in culture supernatant of 005 cells in various conditions. VEGF was released from 005 cells constitutively, and DFO treatment enhanced the production of VEGF significantly in DFS medium and EGM. Data represent mean ± SD of triplicate assays. (*B*) Effect of anti-VEGF NAb on tube formation. The 005 cells cultured in the indicated conditions were seeded on Matrigel, and tube formation was observed after 20 h. We omitted human VEGF from the EGM in this assay and used 1 μg/mL anti-VEGF NAb. (*C*) Effect of anti-VEGF receptor small molecule inhibitor AG28262 on tube formation of 005 cells. We cultured cells and observed tube formation under the same condition indicated in *B*, except for the addition of NAb. (*D*) Survival curve of the GBM mice treated with AG28262. GFAP-Cre transgenic mice received stereotaxic injection of LVs in the hippocampus of the brain. Mice were administrated 100 $mg \cdot kg^{-1} \cdot d^{-1}$ AG28262 orally for 6 wk from the sixth week after lentiviral injection. Control mice were administrated vehicle (0.5% carboxyl methyl cellulose). The survival curve was obtained by the Kaplan–Meier method, and the statistical difference was examined by the log-rank test. (*E*) Frequency of TDEC-forming vessels in the mouse GBM. Tumors were obtained from the mice that developed tumors and examined by immunofluorescence assay using a confocal microscope. Data represent mean ± SD from six (control) or five (AG28262) mice. *<0.5% by the Mann–Whitney *U* test; **<0.5% by the Wilcoxon signed-rank test; NS, not significant by the Wilcoxon signed-rank test.

with GBM to anti-VEGF therapies, we have examined the effect of VEGF receptor inhibitor on tumor development and TDEC formation in vivo using our mouse GBM model. We have administrated the VEGF receptor inhibitor AG28262 from week 6–12 following LV transduction. As shown in Fig. 6*D*, there was no significant difference in survival between the control group and AG28262 group ($P = 0.3688$), indicating that the VEGF inhibitor had almost no effect on tumor growth as observed in clinical studies. Examination of tumor vessels revealed that TDECs increased in the treated mice compared with control mice, however. Although the regular ECs decreased in the treated mice, TDECs significantly increased in ratio compared with control mice (Fig. 6*E*). Furthermore, the increase of TDECs in the AG28262-treated mice was particularly significant in the border area of the tumor, which contains fewer TDECs than the deep area in control mice (Fig. 6*E*). These results indicate that TDEC formation is resistant to the anti-VEGF therapy and strongly suggest the contribution of TDECs in the clinical resistance of GBM to anti-VEGF therapies.

TDECs in Xenograft Tumors of Human GBM Spheres. We next asked if TDECs were also found in human GBMs. We obtained three lenti-GFP–transduced human GBM spheres (21) and transplanted them in the brains of NOD-SCID mice. The resulting tumors examined by immunofluorescence show that regular vascular ECs express vWF but not human nestin or GFP (Fig. 7*A*). In contrast, some ECs express not only vWF but human nestin and GFP (Fig. 7*B*). Fig. 7*C* further shows that regular GFP^- ECs were human CD31 (hCD31)-negative but mouse CD31 (mCD31)-positive, whereas GFP^+ EC cells expressed hCD31 but not mCD31 (Fig. 7*D*). It thus appears that like the mouse GBMs, human GBMs are also capable of forming TDECs. The average ratio of TDECs in total ECs in three transplanted GBMs was 15–44% in the deep area and 4–22% in the border area (Fig. S3). Therefore, as in the mouse model, hypoxia may also play an important role in TDEC formation in human GBMs.

Presence of EGF Receptor-Positive ECs in Clinical Samples of Patients with GBM. Finally, we wanted to determine if direct clinical samples from patients with GBM also contained TDECs. We took advantage of the genetic abnormalities in the form of EGF receptor (EGFR) amplification in these tumors and asked if some ECs contained both human vWF and EGFR. Fig. 7*E* shows the ECs in the normal human brain by immunofluorescence with vWF antigen (Fig. 7*E*, *i*, *iii*, and *iv*) but no reactivity to anti-EGFR antigen (Fig. 7*E*, *ii*, *iii,* and *iv*). In contrast, Fig. 7F shows that some ECs in the clinical tumor sample express both vWF and EGFR (Fig. 7*F i–iv*), offering strong evidence for the presence of TDECs in human GBMs.

Discussion

In tumor angiogenesis, BM-derived circulating endothelial precursors (CEPs) are known to be the main source of the vascular ECs (22). A recent study suggested that the BM-derived CEPs did not contribute to the vascular endothelium, however (23). To date, the presence of TDECs has been suggested in several neoplasias, such as CML, lymphoma, and myeloma, by analyzing clinical samples (8–10). In these tumors, tumor-specific fusion genes resulting from chromosomal translocation were used for the tumor-specific markers. Here, we have demonstrated the presence of blood vessel ECs expressing the tumor marker GFP in our recently developed mouse GBM model, in human GBM xenografts, and clinical samples from patients. In contrast to the conventional theory of tumor angiogenesis in which the ECs are derived from mesodermal BM progenitor cells (22), the presence of TDECs in GBM suggests that the ECs transdifferentiated from the neuroectoderm and that tumor cells can also be involved in tumor angiogenesis. The endothelial transdifferentiation of the tumor cells may result from the aberrant stem cell character of the tumor progenitor cells. The other possible mechanism is that the endothelial differentiation of GBM cells is not the result of transdifferentiation but reflects the normal differentiation pathway of the NSC, which has previously been described to differentiate into ECs (16). If this is also observed in the normal differentiation of human NSCs, perhaps the terminology of transdifferentiation needs reconsideration.

Vasculogenic mimicry (VM) has been reported in melanoma as fluid-conducting channels formed by the tumor cell itself. In contrast to the regular blood vessels, VM lacks ECs; therefore, VM was easily distinguishable from regular blood vessels. VM was also reported in nonmelanoma tumors, including GBM (24–26). The TDECs in this study are likely to be different from the VM because the TDECs are indistinguishable from regular ECs, except for the tumor-specific markers (e.g., GFP) or chromo-

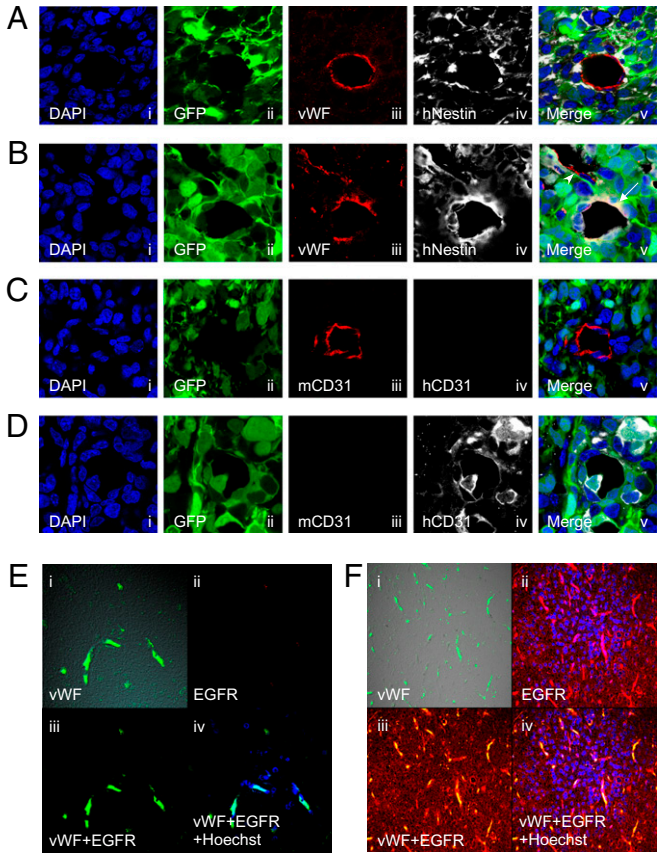

Fig. 7. TDEC formation in a xenograft model using human GBM spheres and patient samples. Representative images of regular ECs (*A* and *C*) and TDECs (*B* and *D*) in brain tumors developed in NOD-SCID mice transplanted with human GBM spheres. (*A*–*D*) (*i*) DAPI nuclear staining; (*ii*) GFP; (*iii*) and (*iv*) expression of indicated antigens; (*v*) merging image. (*A* and *B*) Tumors were stained with anti-vWF antibody, which reacts with both mouse and human vWF, and with an antibody specific for human nestin. (*A*) Regular ECs expressed vWF (*iii*) but not GFP (*ii*) or human nestin (*iv*). (*B*) TDECs expressed vWF (*iii*), GFP (*ii*), and human Nestin (*iv*; *v*, showing the merge with an arrow). A regular EC is indicated by the arrowhead (*v*). (*C* and *D*) Tumors were also stained with antibodies specific for mouse CD31 or human CD31. (*C*) Regular ECs expressed mouse CD31 (*iii*) but not human CD31 (*iv*). (*D*) TDECs expressed human CD31 (*iv*) but not mouse CD31 (*iii*). (*E* and *F*) Representative images of blood vessels of clinical samples of patients with GBM. (*i*) vWF; (*ii*) EGFR; (*iii*) merging image; (*iv*) merging image with Hoechst 33258 nuclear staining. (*E*) Vessels of normal brain expressed vWF (*i*) but not EGFR (*ii*). (*F*) vWF$^+$ ECs (*i*) strongly expressed EGFR (*ii*), and surrounding tumor cells expressed EGFR (*ii*).

somal rearrangements. There is another aberrant tumor vessel, the "mosaic tumor vessel," which was reported in colon cancer (27). The mosaic blood vessels are lumens formed with both ECs and tumor cells lacking EC markers. Because the TDECs are expressing EC markers and behave as regular ECs, the TDECs are likely to be different from the mosaic vessels.

The transdifferentiation of tumor cells into vessel formation in GBM was not previously recognized, probably because of the lack of a good tumor marker. We also suggest that hypoxia is an important factor of endothelial differentiation in addition to regular tumor vessel formation. In the hypoxic condition, induction of VEGF expression through the stabilization of HIF-1α is an important factor for tumor angiogenesis (15). In contrast to regular endothelial differentiation, however, in vitro assays have suggested that the formation of TDECs is independent of VEGF and FGF (Fig. 6 *B* and *C*). In addition, administration of the anti-VEGF receptor inhibitor AG28262 did not improve survival of the GBM mice (Fig. 6*D*), and TDEC formation increased in contrast to regular ECs (Fig. 6*E*). Therefore, the involvement of TDECs in tumor angiogenesis might be one of the resistance mechanisms against anti-VEGF therapies and may require novel combination therapies.

While this paper was under review, two articles (28, 29) were published that further support the notion that a proportion of ECs contributing to the formation of blood vessels in human GBMs originate from tumor cells. The findings of these two groups show that ECs (ranging from 20–90%) in the tumors carry genetic abnormalities found in the tumor cells themselves. Thus, together with the findings reported here, it is clear that part of the vasculature in GBMs originates from tumor cells, bypassing the normal mechanisms of angiogenesis, thus offering an additional therapeutic opportunity to treat the disease.

Materials and Methods

Establishment of Mouse GBM Model by Lentiviral Vector Injection. The mouse GBM model was established as described (13). Briefly, we injected the Cre-inducible LVs Tomo H-RasV12 LV and Tomo AKT LV stereotaxically into the hippocampus of GFAP-Cre/p53$^{+/-}$ transgenic mice. More recently, mouse GBM models have also been generated in GFAP-Cre mice using a single lentiviral vector containing activated H-Ras and sip53. We have killed mice to take tumor samples when the mice show tumor-related signs, such as a domed head, a hunched position, lethargy, and weight loss. In most cases, it takes 3–4 mo after vector injection before tumor-related signs appear.

Cell Culture. Mouse GBM-initiating cell lines 005 and 006 were established as described (13). The 005 and 006 cells were maintained in N2 medium, which contains DMEM/F-12 (Omega Scientific), 1% N2 supplement (Invitrogen), 20 ng/mL human FGF-2 (Peprotech), 20 ng/mL human EGF (Promega), and 40 μg/mL heparin (Sigma). In the differentiation-induction assay, cells were cultured in DFS medium [10% (vol/vol) FBS] or EGM-2 (Lonza). To reproduce the hypoxic condition, we added 100 μg/mL DFO mesylate (Sigma) into the above media. The 005 cells were also cultured in the 2% O_2 condition using an N_2O_2 incubator. Mouse GBM-initiating 005 cells were transplanted into the hippocampus of NOD-SCID mice or DsRed transgenic mice. HUVECs were cultured in the EGM-2.

Transplantation of Mouse GBM-Initiating Cells. Mouse GBM-initiating 005 and 006 cells were transplanted into brains of NOD-SCID mice or DsRed transgenic mice. A total of 3×10^5 cells were suspended in 1–1.5 μL of PBS and injected stereotaxically in the right hippocampus. These mice developed GBM about 1–2 mo after transplantation. In some cases, as few as 5,000 cells were injected, except the tumors took longer to develop.

Immunofluorescence Assay. Mouse brain tumors were processed as described (13). The primary antibodies used in this study are as follows: rabbit anti-vWF (Abcam), rat anti-mCD31 (MEC13.3; Becton Dickinson), rat anti-mCD34 (RAM34; Becton Dickinson), rat anti-mCD144 (11D4.1; Becton Dickinson), chicken anti-nestin (Abcam), rabbit anti-DYKDDDK (Cell Signaling), goat anti-VEGF-R2 (Abcam), and rabbit anti-FGF-R1 (Abcam). The secondary antibodies used were as follows (all from Invitrogen): Alexa Fluor 568 anti-rabbit IgG, Alexa Fluor 568 anti-rat IgG, Alexa Fluor 647 anti-rabbit IgG, Alexa Fluor 647 anti-rat IgG, Alexa Fluor 647 anti-chicken IgG, and Alexa Fluor 647 anti-goat IgG. The nucleus was stained by DAPI. The images were obtained by confocal laser scanning microscopy (TCS SP2 ABS; Leica or LSM 5 PASCAL; Carl Zeiss), and the obtained images were processed by Photoshop software (Adobe).

Hypoxyprobe Assay. To detect hypoxic regions of the brain tumors, a Hypoxyprobe-1 Omni kit (Natural Pharmacia International) was used. We injected 45 mg of Hypoxyprobe-1 into the tail veins of tumor-harboring mice 30 min before euthanasia. Brain sections were stained with rabbit anti-Hypoxyprobe antibody, followed by staining with Alexa Fluor 647-labeled anti-rabbit IgG antibody (Invitrogen). The images were obtained by confocal laser scanning microscopy.

Blood Flow Detection Assay. We injected 50 μg of biotinylated lectin (Vector Laboratories) into the tail veins of tumor-harboring mice 15 min before euthanasia. Brain sections were stained with Alexa Fluor 647-labeled streptavidin (Invitrogen). The images were obtained by confocal laser scanning microscopy.

Flow Cytometry. The brain tumors were dissociated using a Neural Tissue Dissociation Kit (Miltenyi Biotec), and 005 cells were collected after differ-

entiation induction. These cells were stained with the following fluorescence-labeled antibodies: peridinin chlorophyll protein-Cy5.5 anti-mCD45 (30-F11; Becton Dickinson), phycoerythrin (PE) anti-mCD34 (RAM34; Becton Dickinson), Alexa Fluor 647 anti-mCD31 (MEC13.3; BioLegend), and PE anti-mH-2K^d (SF1-1.1; Becton Dickinson). They were then analyzed on a BD LSR I flow cytometer (Becton Dickinson).

Western Blotting. Nuclear proteins from 005 cells cultured in various conditions were extracted and subjected to SDS/PAGE. Proteins were transferred to a PVDF membrane and probed with mouse anti-HIF-1α antibody (Novus), followed by probing with HRP-labeled anti-mouse IgG (Santa Cruz). The blot was reprobed with rabbit anti-lamin B1 antibody (Abcam) and HRP-labeled anti-rabbit IgG (GE Healthcare) after treatment with a ReBlot Plus kit (Millipore). A fluorescence signal was generated using an ECL kit (GE Healthcare).

ELISA. The VEGF concentration of culture supernatant of 005 cells was measured by ELISA using a Duo Set Mouse VEGF kit (R&D Systems). Optical density at 450 nm was measured by an HTS 7000+ microplate reader (Perkin–Elmer).

Tube Formation Assay. The 005 cells cultured in various conditions were seeded on Matrigel (Becton Dickinson). HUVECs were suspended in RPMI 1640 medium supplemented with 1% FBS and seeded on Matrigel in the presence or absence of 10 ng/mL mouse VEGF (mVEGF) and 1 μg/mL anti-mVEGF NAb. After 20 h, images of the cells were taken using an inverted fluorescence microscope (Axiovert 100; Zeiss).

Human GBM Sphere Cultures. The human GBM sphere lines (BT37, BT70, and BT74) were derived from GBM biopsies, implanted into NOD-SCID mice, and passaged serially in mice to maintain authentic biology (30). Dissected xenografts were washed in artificial cerebrospinal fluid and manually dissociated into single cells. Red blood cells were removed using Lympholyte-M (Cedarlane). The cells were cultured in DMEM/F12 (with L-glutamine; Invitrogen) medium containing glucose (0.3%), penicillin/streptomycin (50 μg/mL), Apo-transferrin (0.1 mg/mL), progesterone (20 nM), sodium selenite (30 nM), putrescine (60 μM), insulin (25 μM/mL), sodium bicarbonate (3 mM), Hepes (10 mM), 20 ng/mL EGF, 10 ng/mL leukemia inhibitory factor (LIF), and 20 ng/mL FGF. Live cells were counted using a hemocytometer and trypan blue exclusion.

Lentiviral Transduction. Lentiviral vector stocks of pLKO-GFP lentiviral vectors were produced as previously described (31). For neurosphere transduction, 110 mL of virus was concentrated by ultracentrifugation using an SW-28 rotor (Beckman Coulter) and rotated at 19,500 rpm at 4 °C for 3 h. The pellet was resuspended in 360 μL of serum-free DMEM overnight. Fifty microliters of virus was used to infect 100,000 viable cells.

In Vivo Human Xenograft Model. Animal husbandry was performed according to University of California at San Diego guidelines under Institutional Animal Care and Use Committee-approved protocols. For orthotopic transplants, 2×10^5 cells in 2 μL of HBSS were injected stereotaxically. Mice were killed when morbid, and brain tumors were perfused with PBS and 4% paraformaldehyde (wt/vol), excised, and processed for histological studies.

Human GBM Clinical Samples. We retrospectively reviewed the cases of patients with GBM who were treated at Okayama University Hospital. All tumor samples were fixed with formalin and embedded in paraffin. These samples were approved by the patients for research use. The primary antibodies used in this assay were anti-EGFR antibody (MS-378-P; NeoMarker) and anti-human vWF (A0082; Dako). The secondary antibodies were anti-mouse IgG Cy3 (c-2181; Sigma) and anti-rabbit IgG FITC (F-4890; Sigma). The nucleus was stained by Hoechst 33258. The images were obtained by confocal laser scanning microscopy (LSM510; Zeiss).

ACKNOWLEDGMENTS. We thank Drs. D. Cheresh, F. H. Gage, K. Shimozaki, and H. Kato for useful discussions and Dr. K. Suzuki, G. Estepa, M. Schmitt, B. Coyne, and the other members of the Verma and Gage laboratories of the Salk Institute for help. We also thank Pfizer for AG28262. T.M. was supported by the American Brain Tumor Association. I.M.V. is an American Cancer Society Professor of Molecular Biology and holds the Irwin Mark Jacobs Chair in Exemplary Life Sciences. I.M.V. was supported by the National Institutes of Health (Grant HL053670), National Cancer Institute (Grant P30CA014195), Merieux Foundation, Ellison Medical Foundation, Ipsen/Biomeasure, Sanofi Aventis, and H. N. and Frances C. Berger Foundation. S.K. was supported by the National Institutes of Health (Grants K08CA124804 and 3P30CA023100-25S8) and James S. McDonnell Foundation. M.Y. was supported by the National Cancer Institute (Grant R01CA132971-01A1).

1. Wen PY, Kesari S (2008) Malignant gliomas in adults. *N Engl J Med* 359:492–507.
2. Jain RK, et al. (2007) Angiogenesis in brain tumours. *Nat Rev Neurosci* 8:610–622.
3. Vredenburgh JJ, et al. (2007) Phase II trial of bevacizumab and irinotecan in recurrent malignant glioma. *Clin Cancer Res* 13:1253–1259.
4. Bergers G, Hanahan D (2008) Modes of resistance to anti-angiogenic therapy. *Nat Rev Cancer* 8:592–603.
5. Shojaei F, Ferrara N (2008) Refractoriness to antivascular endothelial growth factor treatment: Role of myeloid cells. *Cancer Res* 68:5501–5504.
6. Pope WB, Lai A, Nghiemphu P, Mischel P, Cloughesy TF (2006) MRI in patients with high-grade gliomas treated with bevacizumab and chemotherapy. *Neurology* 66:1258–1260.
7. Pàez-Ribes M, et al. (2009) Antiangiogenic therapy elicits malignant progression of tumors to increased local invasion and distant metastasis. *Cancer Cell* 15:220–231.
8. Gunsilius E, et al. (2000) Evidence from a leukaemia model for maintenance of vascular endothelium by bone-marrow-derived endothelial cells. *Lancet* 355:1688–1691.
9. Streubel B, et al. (2004) Lymphoma-specific genetic aberrations in microvascular endothelial cells in B-cell lymphomas. *N Engl J Med* 351:250–259.
10. Rigolin GM, et al. (2006) Neoplastic circulating endothelial cells in multiple myeloma with 13q14 deletion. *Blood* 107:2531–2535.
11. Pezzolo A, et al. (2007) Tumor origin of endothelial cells in human neuroblastoma. *J Clin Oncol* 25:376–383.
12. Bussolati B, Grange C, Sapino A, Camussi G (2009) Endothelial cell differentiation of human breast tumour stem/progenitor cells. *J Cell Mol Med* 13:309–319.
13. Marumoto T, et al. (2009) Development of a novel mouse glioma model using lentiviral vectors. *Nat Med* 15:110–116.
14. Dahlstrand J, Collins VP, Lendahl U (1992) Expression of the class VI intermediate filament nestin in human central nervous system tumors. *Cancer Res* 52:5334–5341.
15. Bergers G, Benjamin LE (2003) Tumorigenesis and the angiogenic switch. *Nat Rev Cancer* 3:401–410.
16. Wurmser AE, et al. (2004) Cell fusion-independent differentiation of neural stem cells to the endothelial lineage. *Nature* 430:350–356.
17. Yang M, Reynoso J, Bouvet M, Hoffman RM (2009) A transgenic red fluorescent protein-expressing nude mouse for color-coded imaging of the tumor microenvironment. *J Cell Biochem* 106:279–284.
18. Ivan M, et al. (2001) HIFalpha targeted for VHL-mediated destruction by proline hydroxylation: Implications for O2 sensing. *Science* 292:464–468.
19. Jaakkola P, et al. (2001) Targeting of HIF-alpha to the von Hippel-Lindau ubiquitylation complex by O2-regulated prolyl hydroxylation. *Science* 292:468–472.
20. Zou HY, et al. (2004) AG-028262, a novel selective VEGFR tyrosine kinase antagonist that potently inhibits KDR signaling and angiogenesis in vitro and in vivo. *Proc Am Assoc Cancer Res* 45:A2578.
21. Chen J, et al. (2010) Inhibition of Notch Signaling Blocks Growth of Glioblastoma Cell Lines and Tumor Neurospheres. *Genes Cancer* 1:822–835.
22. Bertolini F, Shaked Y, Mancuso P, Kerbel RS (2006) The multifaceted circulating endothelial cell in cancer: Towards marker and target identification. *Nat Rev Cancer* 6:835–845.
23. Purhonen S, et al. (2008) Bone marrow-derived circulating endothelial precursors do not contribute to vascular endothelium and are not needed for tumor growth. *Proc Natl Acad Sci USA* 105:6620–6625.
24. Hendrix MJ, Seftor EA, Hess AR, Seftor RE (2003) Vasculogenic mimicry and tumour-cell plasticity: Lessons from melanoma. *Nat Rev Cancer* 3:411–421.
25. Yue WY, Chen ZP (2005) Does vasculogenic mimicry exist in astrocytoma? *J Histochem Cytochem* 53:997–1002.
26. El Hallani S, et al. (2010) A new alternative mechanism in glioblastoma vascularization: Tubular vasculogenic mimicry. *Brain* 133:973–982.
27. Chang YS, et al. (2000) Mosaic blood vessels in tumors: Frequency of cancer cells in contact with flowing blood. *Proc Natl Acad Sci USA* 97:14608–14613.
28. Ricci-Vitiani L, et al. (2010) Tumour vascularization via endothelial differentiation of glioblastoma stem-like cells. *Nature* 468:824–828.
29. Wang R, et al. (2010) Glioblastoma stem-like cells give rise to tumour endothelium. *Nature* 468:829–833.
30. Lee J, et al. (2006) Tumor stem cells derived from glioblastomas cultured in bFGF and EGF more closely mirror the phenotype and genotype of primary tumors than do serum-cultured cell lines. *Cancer Cell* 9:391–403.
31. Moffat J, et al. (2006) A lentiviral RNAi library for human and mouse genes applied to an arrayed viral high-content screen. *Cell* 124:1283–1298.